Androgen blockade primes NLRP3 in macrophages to induce tumor phagocytosis

Kiranj Chaudagar[1,8], Srikrishnan Rameshbabu[1,8], Shenglin Mei[2,9], Taghreed Hirz[2,9], Ya-Mei Hu[3,4,5,7,9], Anna Argulian[1], Brian Labadie[1], Kunal Desai[1], Sam Grimaldo[1], Doga Kahramangil[1], Rishikesh Nair[1], Sabina DSouza[1], Dylan Zhou[1], Mingyang Li[1], Farah Doughan[1], Raymond Chen[1], Jordan Shafran[1], Mayme Loyd[1], Zheng Xia[3,4,5,7], David B. Sykes[2], Amy Moran[6,7], Akash Patnaik[1]

[1]Section of Hematology/Oncology, Department of Medicine, University of Chicago, Chicago, IL, USA.

[2]Center for Regenerative Medicine, Massachusetts General Hospital Cancer Center, Boston, MA, USA.

[3]Computational Biology Program, Oregon Health & Science University, Portland, OR, USA.

[4]Department of Biomedical Engineering, Oregon Health & Science University, Portland, OR, USA.

[5]Department of Molecular Microbiology and Immunology, Oregon Health & Science University, Portland, OR, USA.

[6]Department of Cell, Developmental and Cancer Biology, Oregon Health and Science University, Portland, OR, USA.

[7]Knight Cancer Institute, Oregon Health and Science University, Portland, OR, USA.

[8]First authorship is equally shared by these individuals.

[9]These authors have contributed equally.

Running title: Androgen receptor blockade-driven NLRP3 priming

Corresponding Author:

Akash Patnaik, M.D., Ph.D., M.M.Sc.

Knapp Center for Biomedical Discovery, 7152

900 East 57th Street

Chicago, IL 60637

Tel: (773) 734-3519

ABSTRACT:

Immune-based therapies induce a durable remission in a subset of patients across a wide range of malignancies. There is limited efficacy of immunotherapy in metastatic castrate-resistant prostate cancer, manifested by a predominance of immunosuppressive (M2) tumor-associated macrophages (TAM) in the tumor microenvironment (TME). Therefore, therapeutic strategies to overcome TAM-mediated immunosuppression are critically needed in advanced prostate cancer (PC). Here we demonstrate that NLR family pyrin domain containing 3 (NLRP3), an innate immune sensing protein, is highly expressed in TAM from metastatic PC patients treated with standard-of-care androgen deprivation therapy (ADT). Androgen receptor (AR) blockade in TAM upregulates NLRP3 expression, but not inflammasome. Concurrent AR blockade and NLRP3 agonist (BMS-392959) treatment promoted the phagocytosis of cancer cells by M2 TAM. Contrary, BMS-392959 monotherapy was sufficient to enhance phagocytosis of cancer cells in anti-tumor (M1, scarce within TME) TAM, that already had high NLRP3 expression. Critically, combinatorial treatment with ADT and BMS-392959 in a murine model of advanced PC resulted in significant tumor control, with tumor clearance in 55% of mice via TAM phagocytosis. Collectively, our results support the NLRP3 as an AR-regulated “macrophage phagocytic checkpoint”, inducibly expressed in TAM by ADT and activated by NLRP3 agonist treatment, the combination resulting in TAM-mediated phagocytosis and tumor control.

INTRODUCTION:

Approximately 1.4 million men are diagnosed with prostate cancer (PC) annually, which accounts for more than 375,000 annual deaths in the United States[1]. While intensified androgen deprivation therapy (ADT) with or without chemotherapy represents the standard-of-care for metastatic prostate cancer (PC), progression to metastatic castration-resistant prostate cancer (mCRPC) is inevitable, causing significant morbidity and mortality[2,3]. Although there has been unprecedented success of immune checkpoint inhibitor (ICI) therapy within subsets of patients across a range of malignancies[4], efficacy has been limited in mCRPC[5-7]. The tumor microenvironment (TME) in mCRPC is enriched in immunosuppressive tumor-associated macrophages (TAM) and lacks antitumor T effector cells, which is thought to be a critical factor limiting immunotherapy efficacy, including ICI[8-10].

The therapeutic activation of Pattern Recognition Receptors, such as cytosolic NOD-like receptors (NLR) modulate the innate immune system to induce cytokine release, including Type I interferons (IFN), chemokines, and growth factors which results in anti-tumor immune responses[11]. NLR family pyrin domain containing 3 (NLRP3) is a molecular platform for stimulating cleavage of pro-caspase-1 into active caspase-1. This results in activation of IL-1β, IL-18, and Gasdermin D, the latter being a pore-forming protein that facilitates cytokine release and pyroptosis, a form of inflammatory cell death[12]. Successful NLRP3 activation requires the presence of two signals. The first is a priming signal, which induces the nuclear factor kappa B (NF-kB) pathway to upregulate both NLRP3 expression and pro-IL1β. The second, an activation signal, can be initiated by cellular stress signals and the sensing of pathogen and damage-associated molecular patterns (PAMP/DAMP)[12]. The consequence of NLRP3 inflammasome activation on tumorigenesis is complex, and implicated in both pro-tumorigenic[13,14] and anti-

cancer processes[11]. Studies in immunogenic murine models showed that NLRP3 mediated cytokine release can result in IFNγ production and $CD8^+$T cell-dependent tumor regression as well as caspase-1-dependent pyroptosis and inhibition of autophagy in cancer cells[11,15]. Conversely, NLRP3 activation in tumor cells[13] or cancer-associated fibroblasts (CAFs)[14] can result in the recruitment of MDSCs into the TME, thereby promoting tumorigenesis. Furthermore, in primary PC, androgen stimulated NLRP3 expression in cancer cells is associated with worse prognosis, high Gleason score, and greater lymph node metastases[16,17].

Using single cell transcriptomic analysis of patients with metastatic PC (mPC), we demonstrated that NLRP3 is highly expressed in TAM following treatment with ADT. Based on these findings, we hypothesized that androgen axis blockade could enhance NLRP3 expression and potentiate innate immune tumor control in advanced PC. Critically, we discovered that blockade of TAM-intrinsic androgen receptor (AR) activity enhanced NLRP3 expression, but not inflammasome activity in the immunosuppressive (M2) TAM. In contrast, anti-tumor (M1) TAM had high *de novo* NLRP3 expression, regardless of AR activity. The combination of AR blockade and NLRP3 agonism significantly enhanced phagocytosis of cancer cells by M2 TAM, whereas NLRP3 agonist treatment alone was sufficient to induce phagocytosis in M1 TAM. Following AR blockade/NLRP3 agonist combination treatment, all TAM acquired a distinct phenotype with high PD-L1 and CD86 expression, indicative of phagocytic TAM. Critically, NLRP3 agonism in combination with ADT resulted in significant tumor control in an aggressive c-myc driven advanced PC model, with 55% of mice achieving complete tumor clearance, which was abrogated by concurrent clodronate (macrophage depletion) treatment, suggesting TAM phagocytosis as a driver of response. Collectively, our results identify the NLRP3 as an AR-

regulated “macrophage phagocytic checkpoint” that can be inducibly expressed and activated in TAM following ADT and NLRP3 agonist treatment, respectively.

RESULTS:

NLRP3 is highly expressed within TAM of mPC

With the goal of discovering novel therapeutic vulnerabilities in the mPC TME, we investigated NLRP3 expression in patients with metastatic prostate cancer. Here three compartments were sampled from this patient cohort: (1) tumor = bone metastatic (BMET) tumor, (2) involved = bone marrow (BM) at the vertebral level adjacent to tumor site and (3) distal = BM from a different vertebral body distant from the tumor site but within the surgical field, and samples analyzed by single cell-RNA sequencing (scRNAseq)[18]. There was a significant enrichment of NLRP3 expression and inflammasome activity within BMET PC patients, particularly in the myeloid cells, relative to benign BM controls (Fig. 1a, Extended Data Fig. 1a). Among these myeloid populations, NLRP3 expression and inflammasome activity were highest within tumor-inflammatory monocytes (TIM) and tumor-associated macrophages (TAM) at BMET tumor sites, relative to either involved, distal or benign BM controls (Extended Data Fig. 1b). Furthermore, TIM and TAM showed significantly higher NLRP3 expression and inflammasome activity relative to other immune cell populations within BMET TME (Extended Data Fig. 1c, d). Given the significantly increased NLRP3 expression within the TIM and TAM, we analyzed NLRP3 expression within the TIM and TAM populations across 7 cancer types[18]. NLRP3 expression was highest within the TIM and TAM of patients with BMET PC as compared to 6 other cancer types including localized primary PC (pPC, Fig. 1b, Extended Data Fig. 1e). Notably, the inflammasome activity of TIM and TAM was similar in BMET PC and in

pPC (Fig. 1b, Extended Data Fig. 1e), indicating that enhanced NLRP3 expression alone is insufficient to drive inflammasome activation. Collectively, these data demonstrate that NLRP3 expression is specifically increased within cells of the macrophage/monocytic lineage in patients with mPC.

Successful NLRP3 activation requires the presence of two signals. The first is a priming signal, which induces the nuclear factor kappa B (NF-kB) pathway to upregulate both NLRP3 expression and pro-IL1β. The second, an activation signal, can be initiated by PAMP/DAMP[12]. Activation of the NLRP3 inflammasome has been known to induce either pyroptotic cell death and ultimately decrease NLRP3 expressing populations or provide sustained activation of immune cells and subsequent cytokine release[19]. Given that the enhanced NLRP3 expression in mPC relative to other tumor types and relative to untreated pPC did not correlate with enhanced inflammasome activation, we tested the hypothesis that the NLRP3 agonist (BMS-392959) would enhance inflammasome pathway activation in TIM and TAM. We treated immortalized bone marrow derived macrophages (iBMDM, M0-polarized[20]) with BMS`959, and observed a dose-dependent increase in markers of inflammasome formation, including cleaved caspase-1 expression and IL-1β/IL-18 secretion (Extended Data Fig. 2a, b, c). Following treatment with BMS`959, we demonstrated co-localization of NLRP3 with caspase-1 (a marker of NLRP3 inflammasome) by imaging flow cytometry (ImageStream™), and enhanced phagocytosis of prostate cancer cells (Myc-CAP) by iBMDM (Extended Data Fig. 2d, e). These data are "proof-of-concept" that NLRP3 agonism can activate the inflammasome complex, resulting in enhanced anti-cancer phagocytic activity *ex vivo*.

M2 TAM are devoid of NLRP3 inflammasome in prostate cancer

TAMs are heterogenous with respect to their activation and functionality[21] and can be broadly classified as M1 (anti-tumor) and M2 (immunosuppressive). To compare NLRP3 expression between M1 and M2 TAM, we performed flow cytometry and western blot analysis, which revealed higher NLRP3 expression in M1-polarized iBMDM (Extended Data Fig. 3a, b). Using single cell transcriptomic analysis in BMET PC, we found that TAM with high NLRP3 expression also had a higher M1 score as well as a positive correlation between M1-score and inflammasome activity (Fig. 1c). This correlation was not observed in M2 TAM (Fig. 1d).

The murine syngeneic Myc-CAP model of prostate cancer recapitulates the molecular and immunological landscape of advanced PC and is also known to be refractory to ICI[22]. To compare our human patient data to our Myc-CAP murine model, we performed flow cytometry to identify NLRP3-expressing populations in the TME. Consistent with the human PC BMET data (Fig. 1a, b, Extended Data Fig. 1b), we found higher NLRP3 expression within TAM at both early (17-fold) and late (12-fold) phases of tumor growth, when compared to the $CD45^-$ fraction. In addition, Gr-MDSC and $CD4^+$T cells had high NLRP3 expression at both phases of tumor growth while cancer-associated fibroblasts (CAF) demonstrated high NLRP3 expression only at early phase (Extended Data Fig. 4a).

We sought to quantify changes in NLRP3 expression within the Myc-CAP TME following treatment with an NLRP3 agonist at dose mimicking target engagement similar to *in vitro* study. Myc-CAP syngeneic tumors were harvested at 24, 48, and 72 hours following a single intra-tumoral (*it*) dose of BMS`959 to elucidate the dynamics of NLRP3 expression following NLRP3 stimulation. Despite high intrinsic NLRP3 expression in $CD4^+$ T cells, Gr-MDSCs, and TAM in untreated tumors, only the M1 TAM (MHC-$II^+$ TAM, Extended Data Fig. 3a) demonstrated enhanced expression (~3-fold) following BMS`959 treatment (Extended Data

Fig. 4b, middle panel). The frequency of M1 TAM did not decrease following NLRP3 activation within TME. On the other hand, there was an increase in Gr-MDSC infiltration and no change in $CD4^+$T cell frequency with a corresponding decrease in NLRP3 expression within both immune subsets (Extended Data Fig. 4b, middle and lower panels). Collectively, these data demonstrate that M1 TAM retain high expression of NLRP3 following acute NLRP3 agonist treatment *in vivo*, which could potentially contribute to TAM-mediated tumor control.

AR inhibition primes NLRP3 within M2 TAM

We observed enhanced NLRP3 expression within the TAM of mPC, relative to other tumor types and relative to primary PC (Fig. 1b). Since all mPC patients had been treated with ADT (gonadotropin-releasing hormone [GnRH] agonist with or without androgen receptor signaling inhibitor) as compared to patients with primary PC and non-prostate malignancies who did not receive ADT (Fig. 1b, Extended Data Fig. 5), we hypothesized that therapy with AR axis blockade might enhance TAM NLRP3 expression. We correlated AR activity with the NLRP3 expression/inflammasome activity in TAM within a dataset (bulk RNAseq) of patients treated with enzalutamide (AR inhibitor therapy, ARi) for metastatic PC. Correlation analysis demonstrated an inverse correlation of AR activity with NLRP3 expression (Fig. 2a) and with inflammasome activity (Fig. 2b) which was preserved across lymph node, bone, and liver metastases.

We performed a similar analysis of the West Coast Dream Team (WCDT) mCRPC cohort (n=99) who had been treated with enzalutamide or abiraterone and noted a consistent inverse correlation of AR activity with inflammasome activity (Extended Data Fig. 6). Furthermore, we observed a direct correlation between response to pembrolizumab following

enzalutamide progression and high M1 macrophage activity within TME, relative to non-responder subset (Fig. 2c). Collectively, these findings demonstrate an inverse relationship between NLRP3 expression and AR activity, with high NLRP3 expression associated with an M1 signature and a favorable clinical response to ICI in mCRPC. This human bioinformatic analysis credentials NLRP3-expressing TAM as a predictive biomarker for responsiveness to ICI.

Since NLRP3 expression is enhanced following ADT or ARi-treatment, we hypothesized that AR signaling may suppress NLRP3 expression within TAM. To assess the impact of AR blockade on NLRP3 expression and activation within TAM *in vitro*, we performed western blotting on M1 and M2 differentiated iBMDM cultured in charcoal-stripped serum (to mimic ADT), following treatment with the testosterone analogue R1881 and the AR inhibitor enzalutamide. Consistent with the *in vivo* findings, NLRP3 expression increased following ARi treatment in M2 iBMDM, which translated to enhanced inflammasome pathway activation (cleaved caspase-1 expression) in combination with BMS`959 (Fig. 2d). Conversely, there was no increase in NLRP3 expression in the ARi-treated M1 iBMDM, and a paradoxical decrease in cleaved caspase-1 expression with the combination of BMS`959 and ARi (Fig. 2d).

We profiled NLRP3 expressing TAM in Myc-CAP following ADT (degarelix, a GnRH antagonist), and observed an increase in TAM infiltration, particularly M2 TAM within the TME at peri-castration (day 7), early resistant (day 18) and late resistant (day 30) stages (baseline tumor size of 200 mm^3 and untreated tumor size of 2500 mm^3, Fig. 2e). Although there was a lower frequency of M1 TAM (0.22%) relative to M2 TAM (1.58%) within the TME at baseline, we observed higher NLRP3 expressing M1 TAM (0.07%) relative to M2 TAM (0.004%) (Fig. 2f). Degarelix treatment resulted in a significant increase in NLRP3-expressing M2 TAM

(0.01%), but not in M1 TAM (0.09%, Fig. 2f), consistent with *de novo* high NLRP3 expression within M1 TAM and ADT-induced increase in M2 TAM within BMET PC (Fig. 1c, d). Collectively, these data demonstrate that AR blockade can prime NLRP3 expression within the immunosuppressive M2-like TAM, thus creating a therapeutic vulnerability for NLRP3 activation in this immunosuppressive subset (in addition to anti-tumor M1 TAM) within the TME. (Figure 2f).

NLRP3 primed iBMDM phagocytized cancer cells

Repolarization and phagocytosis assays were performed to quantify the impact of ADT-induced NLRP3-primed immunosuppressive M2 macrophages on tumor cell phagocytosis. M1 and M2 iBMDM were treated with ARi, alone and in combination with NLRP3 agonist. Within the M2 iBMDM we observed a higher expression of the suppressive markers, Arg1 and CD206, and a lower expression of activation markers, MHC-II and CD86, as compared to M1 iBMDM (Fig. 3a, Extended Data Fig. 3a, 7a, b). Enzalutamide suppressed Arg1 and CD206 expressions on M2 iBMDM, which was accentuated by concurrent treatment with BMS`959 for 1 hour (Fig. 3a). However, neither enzalutamide, BMS`959 nor their combination increased MHC-II and CD86 on M2 iBMDM (Extended Data Fig. 7a, b), demonstrating that enzalutamide/BMS`959 combination specifically inhibits the immunosuppressive phenotype of M2 iBMDM, but does not polarize them towards anti-tumor M1. Treatment with either single agent or their combination did not alter Arg1, CD206, MHC-II and CD86 expression on M1 iBMDM (Fig. 3a, Extended Data Fig. 7a, b).

BMS`959 treatment for 1-hour or for 24-hours resulted in an increase in phagocytosis of cancer cells within M1 iBMDM, which was not accentuated by concurrent enzalutamide

treatment (Fig. 3b). In contrast, BMS`959 monotherapy (1-hour), singly or in combination with enzalutamide did not enhance phagocytosis of Myc-CAP tumor cells. However, after 24 hours of BMS`959 treatment, we observed enhanced phagocytosis of cancer cells within M2 iBMDM, which was significantly enhanced by ARi, and equivalent to ARi/BMS`959 treated M1 iBMDM (Fig. 3b). Collectively, these data demonstrate that ADT-mediated NLRP3 priming synergizes with NLRP3 agonist treatment to enhance phagocytic killing of cancer cells by immunosuppressive M2 macrophages. Since anti-tumor M1 macrophages are already primed for high NLRP3 expression, enhancement of phagocytosis is achieved with NLRP3 monotherapy alone, obviating the need for ADT-induced NLRP3 priming. As both M1 and M2 macrophages demonstrate enhanced phagocytosis following treatment with ADT and NLRP3 agonist and there is no subsequent change in polarization, we have functionally defined this unique subset as NLRP3-primed phagocytic (NPP) macrophages.

NLRP3-primed phagocytic (NPP) iBMDM express PD-L1 and CD86

We sought to phenotypically characterize NPP iBMDM so that this TAM subset could be investigated *in vivo* following NLRP3 agonism based therapy in the murine Myc-CAP model. Flow cytometric profiling was done using 11 markers (SIRPα, CD16, NLRP3, MHC-II, Arg1, TIM3, PD-L1, CD206, CD86, PD-1, CD64) on NPP iBMDM derived from ARi/BMS`959 treated M1 or M2 iBMDM. We observed PD-L1 and CD86 expressions on NPP iBMDM derived from either M1 or M2 iBMDM following treatment for 24 hours with enzalutamide/BMS`959 combination with subsequent phagocytosis (Fig. 3c), but not after 1 hour treatment or within non-phagocytic M1/M2 iBMDM following 24 hours of treatment (Extended Data Fig. 8a). Surprisingly, NLRP3 expression was not associated with NPP iBMDM (Extended

Data Fig. 8a), which likely reflects dynamic changes in NLRP3 expression following BMS`959 treatment (Extended Data Fig. 4b). PD-L1 and CD86 expression of NPP iBMDM was analyzed following treatment with ARi, BMS`959 or the combination (24 hours) in the absence or presence of co-cultured tumor cells, and selectively in the phagocytic iBMDM or NPP iBMDM. In the absence of tumor cell co-culture, we observed no change in PD-L1 expression on M1/M2 iBMDM following single-agent treatment with enzalutamide or NLRP3 agonist or their combination (Extended Data Fig. 8b). However, PDL1 expression on NPP iBMDM derived from M1/M2 iBMDM significantly increased following ARi and BMS`959 combination treatment (at 24 hours, Fig. 3c, Extended Data Fig. 8c). A similar positive association was observed between NPP iBMDM and CD86 (Fig. 3c), except M1 iBMDM exhibited enhanced CD86 expression following treatment with BMS`959 or in combination with enzalutamide even in absence of co-culture (Extended Data Fig. 8b), and further enhanced following co-culture with tumor cells (Extended Data Fig. 8c). Taken together, these data validate PD-L1 and CD86 as phenotypic biomarkers of NPP iBMDM cells that exhibit enhanced phagocytosis of tumor cells.

Inflammasome mediated cytokine release does not regulate NPP iBMDM phenotype

NLRP3 activation results in the release of IL-1β, IL-18, and Gasdermin D, the latter is a pore-forming protein that facilitates cytokine release and pyroptosis, a form of inflammatory cell death[23]. We used an array to quantify cytokines from ARi/BMS`959-treated (1 hour) M1/M2 iBMDM and asked whether the emergence of NPP iBMDM resulted from NLRP3 inflammasome-mediated cytokine release. At baseline, M1 iBMDM secreted IL-1β, a NLRP3-regulated cytokine[12] and other pro-inflammatory cytokines (IFNα/β/γ, TNFα, GM-CSF, CXCL1, CXCL10, CCL5, IL-6, IL-12p70), which was not observed in M2 iBMDM (Extended Data Fig.

9a), consistent with our findings that M2 TAM lack inflammasome activity. Treatment of M1 iBMDM with BMS`959 monotherapy resulted in an increase in IL-1β secretion, which was suppressed in combination with enzalutamide (Extended Data Fig. 9b). These findings are consistent with the observed decrease in inflammasome activity in M1 iBMDM with enzalutamide/BMS`959 combination treatment, relative to BMS`959 monotherapy (Fig. 2d). While BMS`959/enzalutamide combination therapy increased inflammasome activity in M2 iBMDM (Fig. 2d), this was not accompanied by an increase in IL-1β secretion (Extended Data Fig. 9b). Additionally, enzalutamide decreased secretion of IFNβ and IL-10 from M1 iBMDM, which was partially reversed by BMS`959 addition (Extended Data Fig. 9c, d). Enzalutamide alone or in combination with BMS`959 did not alter secretion of these cytokines from M2 iBMDM (Extended Data Fig. 9c, d). Collectively, these findings highlight an absence of contribution of inflammasome mediated cytokine release to the phagocytic properties of NPP iBMDM.

NPP TAM eradicates cancer *in vivo*

Based on the observed induction of tumor cell phagocytosis *ex vivo* by ADT/NLRP3a-induced NPP iBMDM, we hypothesized that ARi/BMS`959 combination therapy would be therapeutically beneficial in the syngeneic Myc-CAP murine model. Flow cytometric analysis of the untreated Myc-CAP TME revealed 2.1% of TAM, including ~22% PD-L1^{+}NPP TAM and ~15% CD86^{+}NPP TAM (Fig. 4a), suggesting that ~0.4% of NPP TAM are insufficient to control tumor growth.

BMS`959 monotherapy increased the population of NPP TAM (~1.5- and ~2.1-fold with PD-L1 and CD86 expression, respectively) within the TME, while enzalutamide alone did not

(~0.8- and ~0.3-fold, respectively) (Fig. 4a). Consistent with our *in vitro* experiments (Fig. 3a, b, c), degarelix/BMS`959 combination therapy significantly enhanced NPP TAM (PD-L1 and CD86 expressing cells by ~3.3- and ~3.8-fold, respectively) relative to BMS`959 treated group (Fig. 4a), suggesting that a synergistic interaction between degarelix and BMS`959 promotes the accumulation of NPP TAM within the TME. Mice treated with BMS`959 monotherapy demonstrated significant tumor control and improved median survival rate (29 days vs. 14 days in control mice, Fig. 4b and Extended Data Fig. 10a). The combination of degarelix and BMS`959 led to long-term tumor control (>60 days), with 55% of mice achieving complete tumor clearance (Fig. 4b and Extended Data Fig. 10a). Flow cytometric analysis of tumors at endpoint revealed a ~5.6-fold enrichment of NPP TAM in degarelix/BMS`959 treated group relative to untreated (Fig. 4c), highlighting the potential role of NPP TAM in driving the *in vivo* anti-tumor response.

We depleted NPP TAM using liposomal clodronate (which selectively depletes phagocytic TAM), administering it weekly one hour prior to treatment with BMS`959 (Fig. 4c). Concurrent treatment with clodronate reversed the benefit of degarelix/BMS`959 combination, decreasing the median survival from >60 days to ~34 days (Fig. 4b). Notably, no mice exhibited a complete response with the triplet therapy of degarelix/BMS`959/clodronate (Fig. 4b and Extended Data Fig. 10a), thus implicating that NPP TAMs are responsible for the ADT/NLRP3 agonist-induced tumor control *in vivo*.

To assess the possible contribution of tumor cell-intrinsic NLRP3 activation on tumor control, we looked for NLRP3 expression within cancer cells, following treatment with enzalutamide, singly and in combination with NLRP3 agonist. Myc-CAP cells lacked NLRP3 expression at baseline (Extended Data Fig. 10b, left panel), which was unchanged following

enzalutamide, BMS`959 monotherapy or their combination treatment (Extended Data Fig. 10b, right panel). *In vitro* enzalutamide/BMS`959 combination treatment caused a minimal decrease in Myc-CAP proliferation (Extended Data Fig. 10c). Importantly, pre-treatment of Myc-CAP cells with enzalutamide, BMS`959 monotherapy or their combination treatment did not alter their phagocytosis within M1 or M2 iBMDM (Extended Data Fig. 10d), demonstrating that an ADT/NLRP3a-induced tumor extrinsic phagocytic mechanism is responsible for tumor control. Taken together, these data demonstrate that androgens directly suppress NLRP3 expression and downstream activation within immunosuppressive M2 TAM, and its abrogation by AR blockade and NLRP3 agonist combination treatment results in significant NPP TAM-mediated tumor control (Fig. 4d). Given the universality of NLRP3 priming within immunosuppressive M2 TAM with androgen blockade, this approach warrants further clinical investigation in neoadjuvant clinical trials across a wide range of solid malignancies.

DISCUSSION:

Macrophages play an important anti-cancer role via phagocytosis to mount both an innate immune response leading to tumor cell clearance and to stimulate adaptive immunity through presentation of tumor-specific antigens[24]. Various therapeutic strategies have been developed to induce macrophage phagocytosis, either by inhibiting the immunosuppressive TAMs within the TME (e.g., CSF-1 inhibition) or blockade of inhibitory phagocytic checkpoints on tumor cells[25,26]. The latter strategy has demonstrated clinical activity[27,28] and includes agents that target "don't-eat-me" macrophage inhibitory checkpoints (i.e., CD47, MHC-I, CD2 and PD-L1) overexpressed by tumor cells to evade phagocytosis[29]. Here we have described the NLRP3 inflammasome as a novel androgen regulated macrophage phagocytic checkpoint in PC. Our *in vivo* studies demonstrated robust tumor regression in an aggressive murine PC model treated

with combined ARi/NLRP3 agonist via NLRP3-primed phagocytic TAM. This therapeutic combination exploits a novel innate immune approach to inhibit the growth of immunologically cold PC.

AR plays a central role in PC tumorigenesis and AR inhibition induces tumor cell apoptosis, inhibits stemness and proliferation, and inhibits migration and metastasis of tumor cells[30]. Despite an initial response to ARi, PC patients ultimately demonstrate progression and develop mCRPC through various tumor cell-intrinsic mechanisms, including AR gene amplification[31,32], amplification of AR enhancers[33,34], AR gene point mutations[35] and AR splice variants such as AR-V7[36,37]. With respect to tumor cell-extrinsic mechanisms, Moran *et al*. have recently demonstrated that blockade of AR in $CD8^+$ T cells increased IFNy expression, inhibited T cell exhaustion, restored response to anti-PD1 therapy and controlled growth of PC[38]. Our study demonstrates that AR blockade primes NLRP3 in immunosuppressive M2 TAM, and that NLRP3 activation by small molecule NLRP3 agonist treatment controls tumor growth in an advanced murine PC model via the enhancement of phagocytosis. NLRP3 priming did not occur in low AR-expressing M1 TAM following AR blockade therapy. However, M1 TAM demonstrated enhanced phagocytosis following NLRP3 agonist treatment, thus highlighting that the absence of AR expression within activated anti-tumor subpopulations of TAM drives NLRP3 expression, which can be exploited via NLRP3 agonism. Collectively, these findings demonstrate that AR expression suppresses NLRP3 expression and resultant innate immunity within M2 TAM.

Classically, TAM are characterized as either “antitumor” M1 or “immunosuppressive” M2. TAM have a high degree of plasticity and can be classified into subtypes (e.g. TREM2+ macrophages in neurodegenerative disorders, immunosuppressive IL4I1+PD-L1+IDO1+ TAM

in solid tumors) based on transcriptional, metabolic and functional profiling[21,39-41]. Here, we found M1 TAM *de novo* programmed for high NLRP3 expression and AR blockade in subsets of M2 TAM primes NLRP3 expression. Following NLRP3 inflammasome formation via NLRP3 agonist therapy, this subset of NPP TAM phagocytosed cancer cells with corresponding upregulation of PD-L1 and CD86. PDL1 is an immunosuppressive checkpoint that inhibits T cells' antitumor response by binding to its cognate receptor PD1[42]. CD86 is expressed on professional antigen-presenting cells (APC, i.e., dendritic cells, macrophages and B cells), and binds to a costimulatory receptor of CD28 to activate both $CD4^+/CD8^+$T cells[43]. CD86 also binds with inhibitory checkpoint CTLA-4 to inhibit T cell activation[44]. Taken together, these observations demonstrate that PD-L1 and CD86 are predictive biomarkers of treatment response to ADT/NLRP3 agonist combination therapy, and suggest that immuno-oncology combinations with PD-1/CTLA-4 blockade therapy will enhance adaptive anti-tumor immunity above and beyond innate immune activation.

AR signalling is a significant contributor to the growth, metastases and treatment-resistance of melanoma[45-47], lung[48], liver[48], bladder[48] and colorectal cancers[49]. Androgen-mediated sexual dimorphism is associated with superior progression-free survival in BRAF/MEKi-treated female patients and mice with melanoma, relative to males. Furthermore, AR blockade restored the anti-tumor response in male mice by tumor cell-intrinsic/extrinsic mechanisms[47], suggesting a broader impact of ARi treatment on the TME to control cancer growth. In contrast, androgen-driven neutrophil maturation decreases risk of metastases in male melanoma patients and mice. This benefit was attenuated by ARi[46], highlighting that sexual dimorphism is immune cell-context specific, and underscoring the importance of mechanistic studies to elucidate AR biology within different immune cell lineages. In our study, we observed

low baseline NLRP3 expression within TAM of leukemia, liver, lung and pancreatic cancers in the absence of ARi treatment. This observation leads to the tantalizing possibility that ARi can prime NLRP3 within TAM across multiple cancers other than PC, thereby creating a therapeutic vulnerability targetable with an NLRP3 agonist, resulting in TAM-mediated phagocytic tumor control. These concepts warrant further translational/clinical investigation, particularly to determine whether ADT/NLRP3 agonist mediated TAM activation and resultant phagocytosis-mediated tumor control is more effective in male vs. female patients across multiple cancer types.

METHODOLOGY:

Single cell RNA sequencing and bioinformatic analysis in human samples. All human samples were obtained following written informed consent and the studies were conducted in accordance with Declaration of Helsinki ethical guidelines. Bone metastatic (BMET) PC samples (n = 7), BMET non-PC samples (n = 3) and bone marrow from patients with benign inflammation (n = 7) were collected and handled in accordance to protocol approved by the Institutional Review Board (Dana Farber/Harvard Cancer Center protocol 13-416 and Partners protocol 2017P000635/PHS). Following consent, metastatic PC/non-PC patients with vertebral bone metastases and benign bone marrow patients with planned hip replacement surgery underwent biopsies and downstream processing as described previously[18]. Tumor specimens/benign bone marrow were enzymatically dissociated to single cell, treated with ACK lysis buffer to remove erythrocytes and suspended in Media 199 supplemented with 2% FBS. Single cell suspensions were stained with CD235 antibody and DAPI dye, which stains for erythroid progenitors in the bone marrow and dead cells, respectively. Cells negative for both

stains were sorted using BD FACS Aria III instrument equipped with a 100um nozzle (BD Biosciences, San Jose, CA) and further sequenced for RNA by Chromium Controller as per manufacturer protocol (10x Genomics). These published FASTQ files were obtained from GSE143791, and further processed using CellRanger. Human genome-hg19 was considered as the reference genome to generate matrix files containing cell barcodes and transcript counts. To accurately classify cells relative to noise, unique molecular identifiers (UMI) threshold was set at 600, and these well-defined cells were included in downstream analysis. Quality control and data integration were done using Conos[50]. NLRP3 expression per cell was calculated as an average normalized (for cell size) gene expression across different cell subsets. NLRP3 high and low expressing populations were characterized by upper and lower quadrant of cells present in the given cell subsets, respectively. A gene set signature score was used to measure cell states in different cell subsets and conditions. Signature scores were calculated as average expression values of genes in each set. Inflammasome activity, M1/M2-scores in each cell were calculated using three sets of the following genes; 1) AIM2, TRAF6, TXNIP, XIAP, TNFAIP3, BCL2, CASP1, CASP12, CASP4, CARD6, CTSB, CTSV, IL18, IL1A, IL1B, IL18BP, IL33, MYD88, IRF1, IRF3, NFkB1, NFKBID, NFKBIB, NLRP3, PSTPIP1, PTGS2, PYCARD, TIRAP, TNFSF14, TNFSF4; 2) AK3, APOL1, APOL2, APOL3, APOL6, ATF3, BCL2A1, BIRC3, CCL5, CCL15, CCL19, CCL20, CCR7, CHI3L2, CSPG2, CXCL9, CXCL10, CXCL11, ECGF1, EDN1, FAS, GADD45G, HESX1, HSD11B1, HSXIAPAF1, IGFBP4, IL6, IL12B, IL15, IL2RA, IL7R, IL15RA, INDO, INHBA, IRF1, IRF7, OAS2, OASL, PBEF1, PDGFA, PFKFB3, PFKP, PLA1A, PSMA2, PSMB9, PSME2, PTX3, SLC21A15, SLC2A6, SLC31A2, SLC7A5, SPHK1, TNF, TRAIL; and 3) ADK, ALOX15, CA2, CCL13, CCL18, CCL23, CD36, CERK, CHN2, CLECSF13, CTSC, CXCR4, DCL-1, DCSIGN, DECTIN1, EGR2, FGL2, FN1, GAS7,

GPR86, HEXB, HNMT, HRH1, HS3ST1, HS3ST2, IGF1, LIPA, LTA4H, MAF, MRC1, MS4A4A, MS4A6A, MSR1, P2RY14, P2RY5, SEPP1, SLC21A9, SLC38A6, SLC4A7, TGFB1, TGFBR2, TLR5, TPST2, respectively[51]**.** Additionally, we utilized published scRNAseq repository of leukemia[52] (n = 20), liver[53] (n = 8), lung[54] (n = 10), pancreatic[55] (n = 21) and primary prostate cancers[56] (n = 11) to understand NLRP3 expression and inflammasome activity.

Cell lines and culture conditions. iBMDM were a generous gift from the Gajewski Lab (University of Chicago) and cultured in DMEM media containing 10% fetal bovine serum (FBS), 1% penicillin/streptomycin and 1% non-essential amino acids. Myc-CAP cells (ATCC) were cultured in DMEM media containing 10% FBS, 2% L-glutamine and 1% penicillin/streptomycin. To study the specific impact of androgens on downstream readouts of NLRP3 pathway activation and macrophage functionality, androgen enriched (AE) media was generated by adding 10% charcoal-stripped FBS (instead of 10% normal FBS) and R1881 (1 nM) to the above mentioned DMEM media. Cells were treated with AE media for 24 hours to establish androgen regulated response.

M1/M2-polarization. iBMDM had M0-phenotype and were polarized to either M1 or M2 following 24 hours treatment with cytokine cocktails, IFNγ (5 ng/mL) + LPS (200 μg/mL) or IL-4 (20 ng/mL), respectively, and analyzed using flow cytometry for the following markers: SIRPα, CD16, MHC-II, Arg1, TIM-3, PD-L1, CD206, CD86, PD-1, CD64, and NLRP3.

Western blot analysis. iBMDM with M0, M1, M2-phenotypes or Myc-CAP tumor cells were treated with BMS`959 and enzalutamide under normal or AE-media conditions, as indicated in

figure legends. Cells were lysed in RIPA buffer and 30 μg of total protein extracts for each sample underwent sodium dodecyl sulfate-polyacrylamide gel electrophoresis (SDS-PAGE), followed by western blot analysis. These blots were probed for NLRP3, Caspase-1, cleaved caspase-1 and GAPDH.

ELISA assay. iBMDMs were treated with BMS`959 at 1, 5, 10, 50 and 100 μM for 1 hour. Supernatants were collected and analyzed for IL-1β/IL-18 cytokine levels as per manufacturer (Thermofisher) instructions provided in ELISA kits: IL-18 (BMS618); IL-1β (BMS6002).

ImageStream. iBMDM were treated with BMS`959 (10 and 100 μM) for 1 hour and trypsinized, washed with PBS (2x) and stained for NLRP3 and cleaved caspase-1 antibodies as per manufacturer protocol (BD Biosciences; 565575). Cells were analyzed on ImageStream Mark II (Amnis; Luminex) to detect NLRP3 inflammasome formation via assessment of overlapping NLRP3 and cleaved caspase-1 signals.

Murine TME analysis. Experiments were performed in accordance with NIH guidelines and protocol approved by the Institutional Animal Care and Use Committee (IACUC) at University of Chicago. Syngeneic FVB mice that are 10-12-weeks of age (Jackson Laboratory, USA) were inoculated subcutaneously with $1x10^6$ Myc-CAP prostate cancer cells (ATCC, USA) in the right flank region. Once tumors were palpable, vernier caliper was used to monitor tumor growth. Volumetric analysis was performed using following equation; volume (mm^3) = 0.5 x length (mm) x width (mm) x width (mm). To identify *in vivo* NLRP3 expressing cell subsets, untreated Myc-CAP tumors were harvested at early (tumor volume = 200 mm^3, baseline) and late (tumor

volume = 2500 mm^3, untreated) phases of tumor growth. Additionally, syngeneic mice with established Myc-CAP subcutaneous tumors (~200 mm^3) were treated with BMS`959 (0.3 mg/kg, *it*, single dose, NLRP3 agonist, N) for 24, 48 and 72 hours, and tumors harvested to understand dynamic changes in NLRP3 expression with TME. To assess impact of ADT on NLRP3 expression within TME, mice with established Myc-CAP subcutaneous tumors (200 mm^3) were treated with degarelix (0.625 mg/mouse, *sc*, monthly, chemical castration, ADT), and tumors were harvested at peri-castration, early resistance, and late resistance stages (at days 7, 18 and 30, respectively).

To analyze NLRP3 expression in specific cell subsets within the TME, tumor single cell suspensions were centrifuged and incubated for 2 minutes in 1 mL of Ammonium-Chloride-Potassium (ACK) solution to lyse red blood cells. ACK was neutralized with 10 mL of PBS and the cell suspension was centrifuged at 1800 rpm for 5 minutes. The cell pellet was resuspended at density of $1x10^6$ cells/mL in PBS containing either myeloid or lymphoid antibody cocktails. Myeloid antibody cocktails were prepared by resuspending 10 μL of anti-CD45, CD11b, CD11c, Ly6c, Ly6g, MHC-II, F4/80, PD-L1, CD86 antibodies and 1 μL of Ghost-viability dye in 1 mL PBS. Lymphoid antibody cocktails were prepared by resuspending 10 μL of anti-CD45, CD3, CD4, CD8, CD19, FoxP3 antibodies and 1 μL of Ghost-viability dye in 1 mL PBS. After 30 minutes of incubation, stained single cell suspensions were washed with PBS and incubated with fix/perm buffer for 15 minutes. Following fixation, either myeloid or lymphoid antibody cocktail-stained cells were incubated overnight with 1 mL perm buffer containing 1 μg of NLRP3 antibody for intracellular stains. These cells were washed with PBS (2x) and incubated with secondary rabbit antibody (1:200 dilution in 1 mL perm buffer) for 1 hour. After completion of staining process, cells were washed, resuspended in PBS and flow cytometry was performed.

Flow cytometry data were gated for myeloid and lymphoid subsets and their NLRP3 expression status assessed using FlowJo v 10.7 software.

Bulk RNA sequencing and bioinformatic analysis. mCRPC patients (n = 16) who progressed on enzalutamide treatment were enrolled in an investigator-initiated clinical trial (NCT02312557), and underwent baseline metastatic site biopsy collection (n = 3 bone sites, n = 3 liver sites, n = 6 lymph node sites and n = 4 other metastatic sites) at Oregon Health and Science University followed by pembrolizumab treatment (200 mg, every three weeks, 4 cycles). Written informed consent was taken at time of enrollment. The study was approved by the local Human Investigations Committee, and carried out in accordance with Department of Health and Human Services guidelines. Response to therapy was defined by > 25% reduction in Prostate Specific Antigen (PSA), compared to baseline. RNA was isolated from biopsies using Qiagen kit, and sequenced on NextSeq (Illumina). FASTQ raw files were generated by the sequencer, further pre-processed to discard the adaptor sequences using Cutadapt (RRID:SCR_011841), and low-quality reads were eliminated. Next, filtered reads were mapped to the human genome (hg19) using STAR aligner (RRID:SCR_004463). To measure AR regulon activity of each sample, we used the VIPER R package (version 1.16.0)[57]. A log1p-transformed TPM gene expression matrix and a regulatory network (regulome) were used as inputs for single-sample VIPER analysis. The transcriptional regulatory network used in this study was curated from several databases as previously described[58]. NLRP3 expression was analyzed using log-transformed expression profile in each sample. Inflammasome activity (gene list present in the previous scRNAseq section) in each sample was determined using the single-sample gene set enrichment analysis (ssGSEA) implemented in the GSVA with R package (version 1.44.5)[59].

Similarly, inflammasome activity was also analyzed in published West Coast Dream Team (WCDT) human mCRPC mRNA dataset repository[60].

Repolarization assay. M1/M2-polarized iBMDM were treated with BMS`959 (10 μM, 1 hour/24 hours) and enzalutamide (10 μM, 24 hours) under normal or AE-media conditions. Cells were trypsinized, washed with PBS (2x), stained for macrophage activation (MHC-II and CD86), suppression (Arg1 and CD206) markers, and analyzed by flow cytometry.

Phagocytosis assay. M1/M2-polarized iBMDM were treated with BMS`959 (10 μM, 1 hour/24 hours) and enzalutamide (10 μM, 24 hours) under normal or AE-media. Following wash out with PBS (2x), they were co-cultured with CTV dye-stained (1:2000 dilution in PBS) Myc-CAP cells at 2:1 ratio for 1 hour. At the end of phagocytosis, cells were washed twice with PBS and stained with anti-SIRPα, CD16, MHC-II, Arg1, TIM-3, PD-L1, CD206, CD86, PD-1, CD64, and NLRP3 antibodies (1:100 dilution for each) and Ghost-viability dye (1:1000 dilution) in 1 mL PBS. Phagocytic activity of treated iBMDM was assessed by flow cytometry, and calculated by normalizing MFI of CTV dye, relative to indicated control groups in figure legends. PD-L1 and CD86 status was analyzed in these total and phagocytic iBMDM.

To study potential tumor cell-intrinsic contribution of androgen blockade/NLRP3 agonist combination therapy on phagocytosis, Myc-CAP cells were treated with BMS`959 (10 μM, 24 hours) and enzalutamide (10 μM, 24 hours) under normal or AE-media. Following treatment, cells were stained with CTV dye, and co-cultured with M1/M2-polarized macrophages at 2:1 ratio for 1 hour. Phagocytic activity of iBMDM were assessed using flow cytometry as described above.

Cytokine array. M1/M2-polarized iBMDM were treated with BMS`959 (10 μM, 1 hour) and enzalutamide (10 μM, 24 hours) under normal or AE-media. Supernatants were collected and analyzed using LGENDplex with macrophage 13-plexinflammatory panel.

Murine prostate tumor growth kinetic and survival analysis. To assess anti-tumor responses, syngeneic mice with established Myc-CAP tumors (200 mm^3) were treated with either BMS`959 (0.3 mg/kg, *it*, weekly, NLRP3 agonist, N), degarelix (0.625 μg/mouse, *sc*, monthly, chemical castration, ADT) or their combination. Tumor growth was monitored using vernier caliper for indicated timepoints in figure legends. Mice were monitored for survival from establishment of Myc-CAP tumors (~200 mm^3) until pre-specified cut-offs for either tumor volume (~2500 mm^3) or treatment duration (60 days) in both treated and untreated groups. After mice reached survival endpoint, tumors were harvested for TME analysis using flow cytometry. For acute mechanistic studies, mice with established Myc-CAP tumors were treated with above mentioned agents or their combination for 7 days. Tumors were harvested and single cell suspensions were processed for TME analysis using flow cytometry, as described in above section.

***In vivo* macrophage depletion studies.** To elucidate the role of macrophages in driving anti-tumor responses *in vivo*, syngeneic mice with established Myc-CAP tumors (200 mm^3) were treated concurrently with clodronate (200 μg/mouse, *ip*, once weekly, Cl), which is known to deplete phagocytic macrophages *in vivo*[61], singly or in combination with degarelix (0.625 μg/mouse, *sc*, monthly, ADT) plus BMS`959 (0.3 mg/kg, *it*, weekly, N) or BMS`959

monotherapy. Prostate tumor growth kinetics and TME analysis were done, as previously described.

Proliferation assay. Myc-CAP cells were treated with BMS`959 (10 μM, 72 hours) and enzalutamide (10 μM, 72 hours) under normal or AE-media conditions. Adherent cells were trypsinized and total number of cells per well counted using hemocytometer. Proliferation rate was calculated by dividing the number of cells at a given time point with the seeding density.

Data Analysis. Data analysis was done using Graph Pad Prism v7. Statistical analysis was done using one way analysis of variance (ANOVA) and Bonferroni post-test with $p<0.05$ level of significance. Unpaired t-tests were used to compare the means between two independent groups. For scRNAseq, NLRP3 expression and inflammasome activity within each cell subset were represented using Uniform Manifold Approximation and Projection (UMAP) method at single cell level. Group comparison for human data were done using Wilcoxon rank-sum tests (for two groups) or Kruskal–Wallis tests (> than two groups). Correlation analysis was done by Pearson test between two continuous variables.

REFERENCES:

1 Sung, H. *et al.* Global Cancer Statistics 2020: GLOBOCAN Estimates of Incidence and Mortality Worldwide for 36 Cancers in 185 Countries. *CA Cancer J Clin* **71**, 209-249, doi:10.3322/caac.21660 (2021).

2 Li, Y., Malapati, S., Lin, Y. T. & Patnaik, A. An integrative approach for sequencing therapies in metastatic prostate cancer. *The American Journal of Hematology/Oncology* **13**, 26-31 (2017).

3 Thomas, T. S. & Pachynski, R. K. Treatment of Advanced Prostate Cancer. *Mo Med* **115**, 156-161 (2018).

4 Robert, C. A decade of immune-checkpoint inhibitors in cancer therapy. *Nature Communications* **11**, 3801, doi:10.1038/s41467-020-17670-y (2020).

5 Heidegger, I. *et al.* A Systematic Review of the Emerging Role of Immune Checkpoint Inhibitors in Metastatic Castration-resistant Prostate Cancer: Will Combination Strategies Improve Efficacy? *Eur Urol Oncol* **4**, 745-754, doi:10.1016/j.euo.2020.10.010 (2021).

6 Sharma, P. *et al.* Initial results from a phase II study of nivolumab (NIVO) plus ipilimumab (IPI) for the treatment of metastatic castration-resistant prostate cancer (mCRPC; CheckMate 650). *Journal of Clinical Oncology* **37**, 142-142, doi:10.1200/JCO.2019.37.7_suppl.142 (2019).

7 Beer, T. M. *et al.* Randomized, Double-Blind, Phase III Trial of Ipilimumab Versus Placebo in Asymptomatic or Minimally Symptomatic Patients With Metastatic Chemotherapy-Naive Castration-Resistant Prostate Cancer. *J Clin Oncol* **35**, 40-47, doi:10.1200/jco.2016.69.1584 (2017).

8 Wang, G., Zhao, D., Spring, D. J. & DePinho, R. A. Genetics and biology of prostate cancer. *Genes Dev* **32**, 1105-1140, doi:10.1101/gad.315739.118 (2018).

9 Almeida, D. V. P. d., Fong, L., Rettig, M. B. & Autio, K. A. Immune Checkpoint Blockade for Prostate Cancer: Niche Role or Next Breakthrough? *American Society of Clinical Oncology Educational Book*, e89-e106, doi:10.1200/edbk_278853 (2020).

10 Stultz, J. & Fong, L. How to turn up the heat on the cold immune microenvironment of metastatic prostate cancer. *Prostate Cancer Prostatic Dis* **24**, 697-717, doi:10.1038/s41391-021-00340-5 (2021).

11 Ghiringhelli, F. *et al.* Activation of the NLRP3 inflammasome in dendritic cells induces IL-1beta-dependent adaptive immunity against tumors. *Nat Med* **15**, 1170-1178, doi:10.1038/nm.2028 (2009).

12 He, Y., Hara, H. & Nunez, G. Mechanism and Regulation of NLRP3 Inflammasome Activation. *Trends Biochem Sci* **41**, 1012-1021, doi:10.1016/j.tibs.2016.09.002 (2016).

13 Theivanthiran, B. *et al.* A tumor-intrinsic PD-L1/NLRP3 inflammasome signaling pathway drives resistance to anti-PD-1 immunotherapy. *J Clin Invest* **130**, 2570-2586, doi:10.1172/JCI133055 (2020).

14 Ershaid, N. *et al.* NLRP3 inflammasome in fibroblasts links tissue damage with inflammation in breast cancer progression and metastasis. *Nat Commun* **10**, 4375, doi:10.1038/s41467-019-12370-8 (2019).

15 Wei, Q., Zhu, R., Zhu, J., Zhao, R. & Li, M. E2-Induced Activation of the NLRP3 Inflammasome Triggers Pyroptosis and Inhibits Autophagy in HCC Cells. *Oncol Res* **27**, 827-834, doi:10.3727/096504018X15462920753012 (2019).

16 Xu, Z. *et al.* NLRP3 inflammasome promoted the malignant progression of prostate cancer via the activation of caspase-1. *Cell Death Discov* **7**, 399, doi:10.1038/s41420-021-00766-9 (2021).

17 Zhao, A. N. *et al.* Disturbing NLRP3 acetylation and inflammasome assembly inhibits androgen receptor-promoted inflammatory responses and prostate cancer progression. *Faseb j* **36**, e22602, doi:10.1096/fj.202200673RRR (2022).

18 Kfoury, Y. *et al.* Human prostate cancer bone metastases have an actionable immunosuppressive microenvironment. *Cancer Cell* **39**, 1464-1478 e1468, doi:10.1016/j.ccell.2021.09.005 (2021).

19 Sharma, B. R. & Kanneganti, T. D. NLRP3 inflammasome in cancer and metabolic diseases. *Nat Immunol* **22**, 550-559, doi:10.1038/s41590-021-00886-5 (2021).

20 De Nardo, D., Kalvakolanu, D. V. & Latz, E. Immortalization of Murine Bone Marrow-Derived Macrophages. *Methods Mol Biol* **1784**, 35-49, doi:10.1007/978-1-4939-7837-3_4 (2018).

21 Locati, M., Curtale, G. & Mantovani, A. Diversity, Mechanisms, and Significance of Macrophage Plasticity. *Annu Rev Pathol* **15**, 123-147, doi:10.1146/annurev-pathmechdis-012418-012718 (2020).

22 Shen, Y. C. *et al.* Combining intratumoral Treg depletion with androgen deprivation therapy (ADT): preclinical activity in the Myc-CaP model. *Prostate Cancer Prostatic Dis* **21**, 113-125, doi:10.1038/s41391-017-0013-x (2018).

23 Shi, J. *et al.* Cleavage of GSDMD by inflammatory caspases determines pyroptotic cell death. *Nature* **526**, 660-665, doi:10.1038/nature15514 (2015).

24 Gajewski, T. F., Schreiber, H. & Fu, Y. X. Innate and adaptive immune cells in the tumor microenvironment. *Nat Immunol* **14**, 1014-1022, doi:10.1038/ni.2703 (2013).

25 Mantovani, A., Allavena, P., Marchesi, F. & Garlanda, C. Macrophages as tools and targets in cancer therapy. *Nat Rev Drug Discov* **21**, 799-820, doi:10.1038/s41573-022-00520-5 (2022).

26 Tap, W. D. *et al.* Pexidartinib versus placebo for advanced tenosynovial giant cell tumour (ENLIVEN): a randomised phase 3 trial. *Lancet* **394**, 478-487, doi:10.1016/s0140-6736(19)30764-0 (2019).

27 Sallman, D. A. *et al.* The first-in-class anti-CD47 antibody Hu5F9-G4 is active and well tolerated alone or with azacitidine in AML and MDS patients: Initial phase 1b results. *Journal of Clinical Oncology* **37**, 7009-7009, doi:10.1200/JCO.2019.37.15_suppl.7009 (2019).

28 Daver, N. *et al.* Phase I/II Study of Azacitidine (AZA) with Venetoclax (VEN) and Magrolimab (Magro) in Patients (pts) with Newly Diagnosed (ND) Older/Unfit or High-Risk Acute Myeloid Leukemia (AML) and Relapsed/Refractory (R/R) AML. *Blood* **140**, 141-144, doi:10.1182/blood-2022-170188 (2022).

29 Wang, Y., Johnson, K. C. C., Gatti-Mays, M. E. & Li, Z. Emerging strategies in targeting tumor-resident myeloid cells for cancer immunotherapy. *J Hematol Oncol* **15**, 118, doi:10.1186/s13045-022-01335-y (2022).

30 Dai, C., Heemers, H. & Sharifi, N. Androgen Signaling in Prostate Cancer. *Cold Spring Harb Perspect Med* **7**, doi:10.1101/cshperspect.a030452 (2017).

31 Abida, W. *et al.* Genomic correlates of clinical outcome in advanced prostate cancer. *Proc Natl Acad Sci U S A* **116**, 11428-11436, doi:10.1073/pnas.1902651116 (2019).

32 Robinson, D. *et al.* Integrative clinical genomics of advanced prostate cancer. *Cell* **161**, 1215-1228, doi:10.1016/j.cell.2015.05.001 (2015).

33 Chen, W. S. *et al.* Genomic Drivers of Poor Prognosis and Enzalutamide Resistance in Metastatic Castration-resistant Prostate Cancer. *Eur Urol* **76**, 562-571, doi:10.1016/j.eururo.2019.03.020 (2019).

34 Quigley, D. A. *et al.* Genomic Hallmarks and Structural Variation in Metastatic Prostate Cancer. *Cell* **174**, 758-769.e759, doi:10.1016/j.cell.2018.06.039 (2018).

35 Veldscholte, J. *et al.* A mutation in the ligand binding domain of the androgen receptor of human LNCaP cells affects steroid binding characteristics and response to anti-androgens. *Biochem Biophys Res Commun* **173**, 534-540, doi:10.1016/s0006-291x(05)80067-1 (1990).

36 Dehm, S. M., Schmidt, L. J., Heemers, H. V., Vessella, R. L. & Tindall, D. J. Splicing of a novel androgen receptor exon generates a constitutively active androgen receptor that mediates prostate cancer therapy resistance. *Cancer Res* **68**, 5469-5477, doi:10.1158/0008-5472.Can-08-0594 (2008).

37 Hu, R. *et al.* Ligand-independent androgen receptor variants derived from splicing of cryptic exons signify hormone-refractory prostate cancer. *Cancer Res* **69**, 16-22, doi:10.1158/0008-5472.Can-08-2764 (2009).

38 Guan, X. *et al.* Androgen receptor activity in T cells limits checkpoint blockade efficacy. *Nature* **606**, 791-796, doi:10.1038/s41586-022-04522-6 (2022).

39 Mantovani, A., Marchesi, F., Malesci, A., Laghi, L. & Allavena, P. Tumour-associated macrophages as treatment targets in oncology. *Nat Rev Clin Oncol* **14**, 399-416, doi:10.1038/nrclinonc.2016.217 (2017).

40 Bian, Z. *et al*. Deciphering human macrophage development at single-cell resolution. *Nature* **582**, 571-576, doi:10.1038/s41586-020-2316-7 (2020).

41 Mulder, K. *et al.* Cross-tissue single-cell landscape of human monocytes and macrophages in health and disease. *Immunity* **54**, 1883-1900.e1885, doi:10.1016/j.immuni.2021.07.007 (2021).

42 Sun, C., Mezzadra, R. & Schumacher, T. N. Regulation and Function of the PD-L1 Checkpoint. *Immunity* **48**, 434-452, doi:10.1016/j.immuni.2018.03.014 (2018).

43 Esensten, J. H., Helou, Y. A., Chopra, G., Weiss, A. & Bluestone, J. A. CD28 Costimulation: From Mechanism to Therapy. *Immunity* **44**, 973-988, doi:10.1016/j.immuni.2016.04.020 (2016).

44 Qureshi, O. S. *et al.* Trans-endocytosis of CD80 and CD86: a molecular basis for the cell-extrinsic function of CTLA-4. *Science* **332**, 600-603, doi:10.1126/science.1202947 (2011).

45 Ma, M. *et al.* Sustained androgen receptor signaling is a determinant of melanoma cell growth potential and tumorigenesis. *J Exp Med* **218**, doi:10.1084/jem.20201137 (2021).

46 Markman, J. L. *et al*. Loss of testosterone impairs anti-tumor neutrophil function. *Nat Commun* **11**, 1613, doi:10.1038/s41467-020-15397-4 (2020).

47 Vellano, C. P. *et al.* Androgen receptor blockade promotes response to BRAF/MEK-targeted therapy. *Nature* **606**, 797-803, doi:10.1038/s41586-022-04833-8 (2022).

48 Chang, C., Lee, S. O., Yeh, S. & Chang, T. M. Androgen receptor (AR) differential roles in hormone-related tumors including prostate, bladder, kidney, lung, breast and liver. *Oncogene* **33**, 3225-3234, doi:10.1038/onc.2013.274 (2014).

49 Roshan, M. H., Tambo, A. & Pace, N. P. The role of testosterone in colorectal carcinoma: pathomechanisms and open questions. *EPMA J* **7**, 22, doi:10.1186/s13167-016-0071-5 (2016).

50 Barkas, N. *et al.* Joint analysis of heterogeneous single-cell RNA-seq dataset collections. *Nat Methods* **16**, 695-698, doi:10.1038/s41592-019-0466-z (2019).

51 Chaudagar, K. *et al.* Reversal of lactate and PD-1-mediated macrophage immunosuppression controls growth of PTEN/p53-deficient prostate cancer. *Clin Cancer Res* **29**, 1952–1968 (2023).

52 Witkowski, M. T. *et al.* Extensive Remodeling of the Immune Microenvironment in B Cell Acute Lymphoblastic Leukemia. *Cancer Cell* **37**, 867-882 e812, doi:10.1016/j.ccell.2020.04.015 (2020).

53 Zhang, Q. *et al.* Landscape and Dynamics of Single Immune Cells in Hepatocellular Carcinoma. *Cell* **179**, 829-845 e820, doi:10.1016/j.cell.2019.10.003 (2019).

54 Lambrechts, D. *et al.* Phenotype molding of stromal cells in the lung tumor microenvironment. *Nat Med* **24**, 1277-1289, doi:10.1038/s41591-018-0096-5 (2018).

55 Peng, J. *et al.* Single-cell RNA-seq highlights intra-tumoral heterogeneity and malignant progression in pancreatic ductal adenocarcinoma. *Cell Res* **29**, 725-738, doi:10.1038/s41422-019-0195-y (2019).

56 Chen, S. J. *et al.* Single-cell analysis reveals transcriptomic remodellings in distinct cell types that contribute to human prostate cancer progression. *Nat Cell Biol* **23**, doi:10.1038/s41556-020-00613-6 (2021).

57 Alvarez, M. J. *et al*. Functional characterization of somatic mutations in cancer using network-based inference of protein activity. *Nat Genet* **48**, 838-+, doi:10.1038/ng.3593 (2016).

58 Guan, X. N. *et al.* Androgen receptor activity in T cells limits checkpoint blockade efficacy. *Nature* **606**, 791-+, doi:10.1038/s41586-022-04522-6 (2022).

59 Hanzelmann, S., Castelo, R. & Guinney, J. GSVA: gene set variation analysis for microarray and RNA-Seq data. *Bmc Bioinformatics* **14**, doi:10.1186/1471-2105-14-7 (2013).

60 Aggarwal, R. *et al*. Targeting Adaptive Pathways in Metastatic Treatment-Resistant Prostate Cancer: Update on the Stand Up 2 Cancer/Prostate Cancer Foundation-Supported West Coast Prostate Cancer Dream Team. *Eur Urol Focus* **2**, 469-471, doi:10.1016/j.euf.2016.10.011 (2016).

61 Chaudagar, K. *et al.* Reversal of Lactate and PD-1-mediated Macrophage Immunosuppression Controls Growth of PTEN/p53-deficient Prostate Cancer. *Clin Cancer Res* **29**, 1952-1968, doi:10.1158/1078-0432.CCR-22-3350 (2023).

Figures:

Figure 1

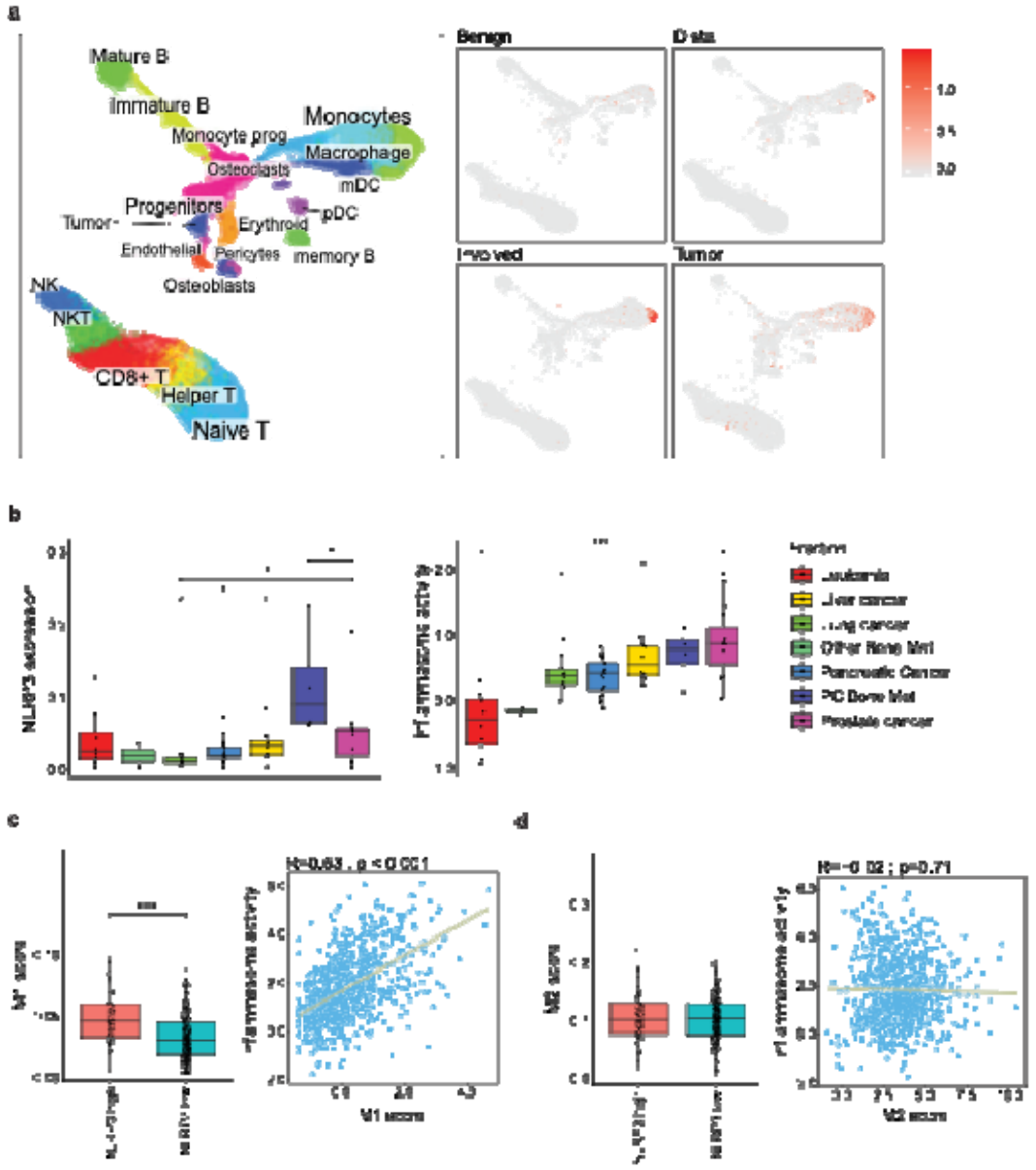

Fig. 1 | NLRP3 expression is enhanced in tumor-associated macrophages (TAM) of ADT-treated metastatic PC patients. a-d, Single cell RNAseq (scRNAseq) was performed on biopsies collected from tumor, involved and distant sites of bone metastatic prostate cancer (BMET PC) patients as described in the Methods section, and compared with healthy benign bone marrow. **a**, UMAP plots represent cell subpopulations within the tumor microenvironment (left) and NLRP3 expression (right) in different sample fractions. **b**, Boxplots show NLRP3 expression and inflammasome activity within TAM across 7 different cancer types listed in the panel. **c-d**, BMET PC TAM were stratified into two groups based on the NLRP3 expression (NLRP3-high: top 25% versus NLRP3-low: bottom 25% TAM). They were further scored for M1 (**c**) and M2 (**d**) phenotypes and correlated with inflammasome activity. Data obtained from specimens of BMET PC (n = 7 patients) for panel **a-d**, healthy benign bone marrow (n = 7 human donors) for panel **a**, leukemia (n = 20 patients), liver cancer (n = 8 patients), lung cancer (n = 10 patients), pancreatic cancer (n = 21 patients), other bone met (non-prostate bone metastatic cancers, n = 3 patients) and primary prostate cancer patients (n = 11 patients) for panel **b**. Except panel **a**, all panels show biological replicates as mean $\pm$ s.e. Significances Significances/p-values were calculated by Wilcoxon rank-sum test (panel **b**, **c, d**) and indicates as follows, *p<0.05, **p<0.01, ***p<0.001 and ****p<0.0001.

Figure 2

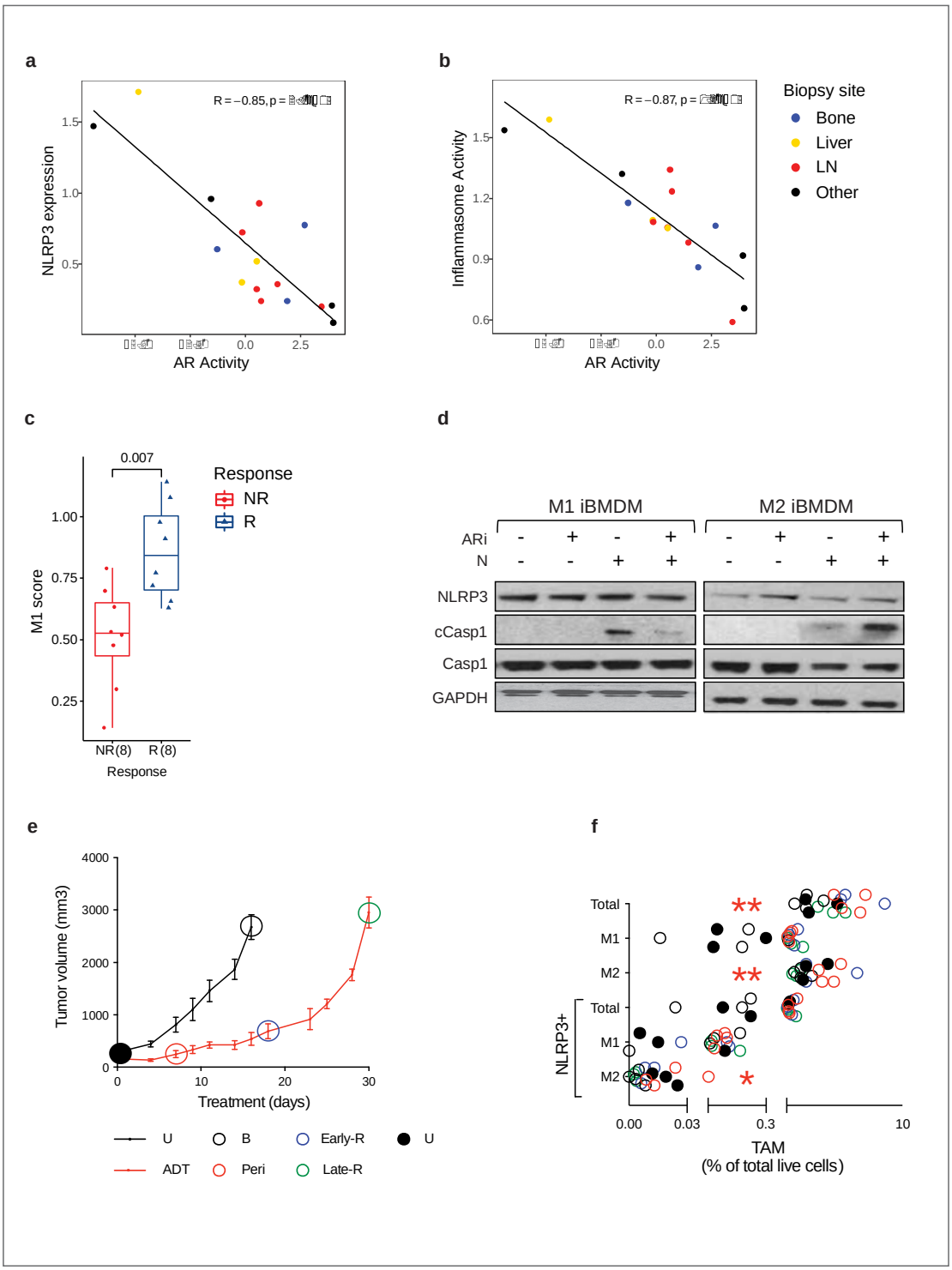
a
R = −0.85, p =
NLRP3 expression
1.5
1.0
0.5
0.0
2.5
AR Activity
b
R = −0.87, p =
Inflammasome Activity
1.5
1.2
0.9
0.6
0.0
2.5
AR Activity
Biopsy site
Bone
Liver
LN
Other
c
0.007
M1 score
1.00
0.75
0.50
0.25
NR (8)
R (8)
Response
Response
NR
R
d
M1 iBMDM
M2 iBMDM
ARi
N
NLRP3
cCasp1
Casp1
GAPDH
e
Tumor volume (mm3)
4000
3000
2000
1000
0
0
10
20
30
Treatment (days)
U
ADT
B
Peri
Early-R
Late-R
U
f
Total
M1
M2
Total
M1
M2
NLRP3+
**
**
*
0.00
0.03
0.3
10
TAM
(% of total live cells)

Fig. 2 | AR blockade primes NLRP3 in immunosuppressive M2 macrophages, but not in anti-tumor M1 macrophages. a-c, Patients with mCRPC who had previously progressed on enzalutamide were treated with pembrolizumab (anti-PD1 antibody) in the context of an investigator-initiated clinical trial (NCT02312557). Bulk RNAseq on baseline metastatic biopsy samples from enzalutamide-refractory mCRPC patients prior to pembrolizumab treatment was utilized to correlate AR activity with NLRP3 expression (**a**)/inflammasome activity (**b**) presented by scatter plots. **c**, The mCRPC patients were stratified into responder (R) *vs* non-responder (NR) groups based on PSA response as described in the Methods section, and the M1 score estimated using bulk RNAseq. **d**, iBMDM were differentiated into M1 and M2 phenotypes using cytokine cocktail, as described in Methods section, and treated with enzalutamide (ARi, 10μM, 24 hours), BMS`959 (N, 10μM, 1 hour) or their combination. The indicated markers of inflammasome expression/activation were probed by western blotting. **e**, Myc-CAP tumors (~200 mm^3, baseline, B) were treated with degarelix (ADT, 0.625μg, *sc*), and harvested at peri-castration (peri, 7 days), early-resistant (early-R, 18 days) and late-resistant (late-R, 30 days) stages following ADT, along with untreated tumors (~2500 mm^3, U). **f**, The harvested tumors were profiled using flow cytometry to assess total and NLRP3-expressing TAM frequency within TME. Data obtained from specimens of metastatic PC (n = 16 patients) for panel **a**, **b**, **c**, biologically independent *in vitro* studies (n = 3 experiments) in the panel **d** and specimens of mice ($n \geq 3$ mice per group) in the panel **e**, **f**. Except panel **d**, all panels show biological replicates as mean $\pm$ s.e. Significances/p-values were calculated by two-way ANOVA test (panel **f**), Kruskal-Wallis test (panel **a**, **b**, **c**) and indicates as follows, *$p<0.05$, **$p<0.01$ and ***$p<0.001$.

Figure 3

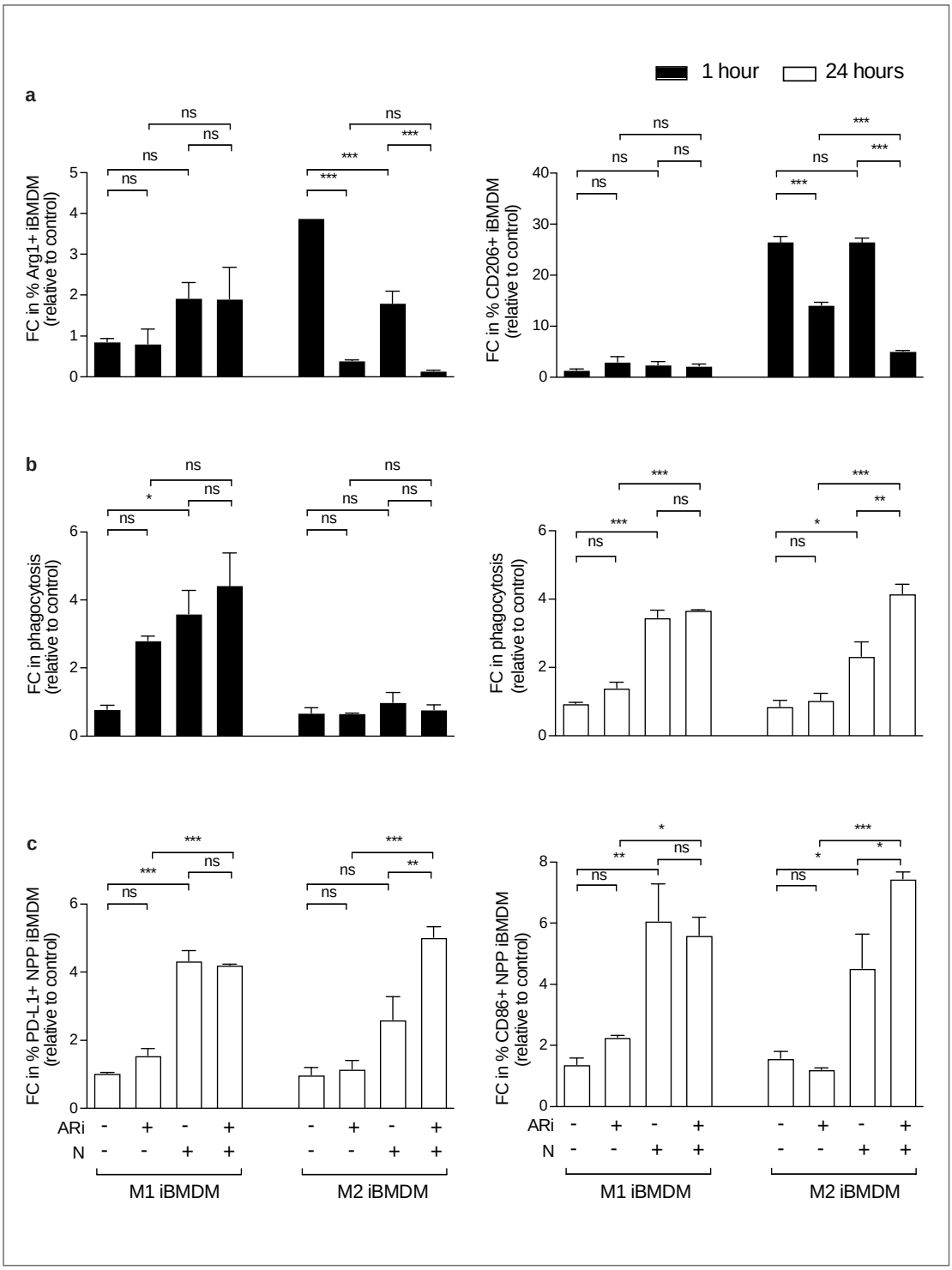
1 hour
24 hours
a
FC in % Arg1+ iBMDM (relative to control)
FC in % CD206+ iBMDM (relative to control)
b
FC in phagocytosis (relative to control)
c
FC in % PD-L1+ NPP iBMDM (relative to control)
FC in % CD86+ NPP iBMDM (relative to control)
ARi
N
M1 iBMDM
M2 iBMDM

Fig. 3 | *In vitro* AR blockade/NLRP3 agonist treatment of M1/M2 iBMDM induces phagocytic uptake of Myc-CAP tumor cells by NLRP3 primed phagocytic (NPP) iBMDM. **a**, iBMDM were differentiated into M1 and M2 phenotypes using cytokine cocktail, as described in the Methods section and treated with enzalutamide (ARi, 10μM, 24 hours), BMS`959 (N, 10μM, 1 hour), or their combination. Flow cytometry was performed to identify Arg1 and CD206 expressing iBMDM. **b**, M1/M2 iBMDM were treated with enzalutamide (ARi, 10μM, 24 hours), BMS`959 (N, 10μM, 1 hour or 24 hours) or their combination and co-cultured with CTV-dye stained Myc-CAP cells for 1 hour, and flow cytometry were performed to determine CTV-dye^{+}iBMDM (indicative of phagocytosis). **c**, NPP iBMDM were identified using flow cytometry for PD-L1 and CD86 expression. Data obtained from the biologically independent *in vitro* studies (n = 3 experiments). All panels show biological replicates as mean ± s.e. Significances/p-values were calculated by one-way ANOVA and indicates as follows, *$p<0.05$, **$p<0.01$ and ***$p<0.001$; ns = not statistically significant. FC = fold change. Control = untreated M1 iBMDM group.

Figure 4

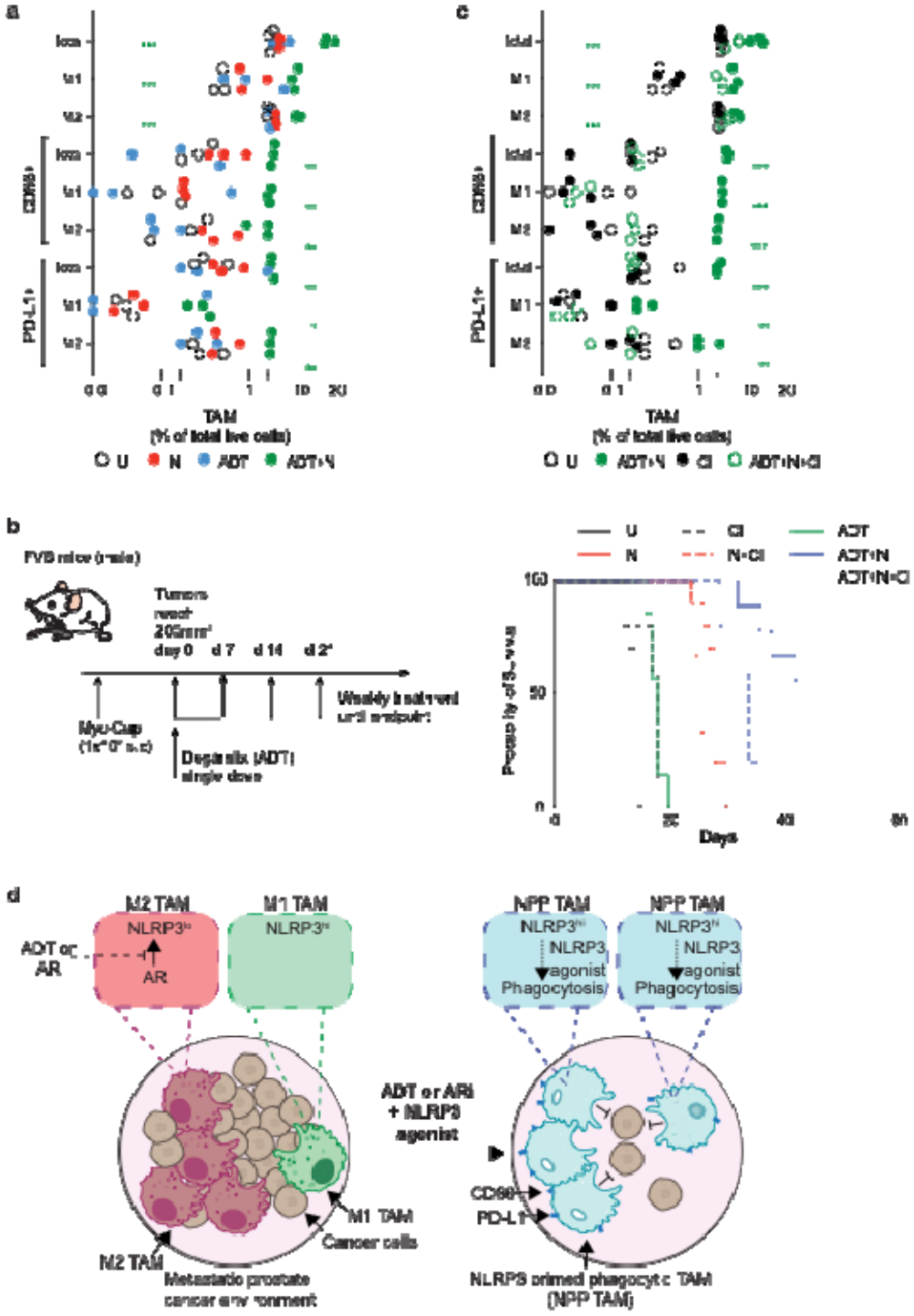
a
c
b
d
TAM
(% of total live cells)
U
N
ADT
ADT+N
CI
ADT+N+CI
Days
M2 TAM
M1 TAM
NLRP3
AR
ADT or AR
ADT or ARi
+ NLRP3
agonist
Phagocytosis
CD86
PD-L1
Cancer cells
Metastatic prostate
cancer environment
NLRP3 primed phagocytic TAM
(NPP TAM)

Fig. 4 | AR blockade/NLRP3 agonist-induced NLRP3 primed phagocytic-tumor associated macrophages (NPP) TAM drive tumor clearance in the majority of Myc-CAP tumor-bearing syngeneic mice. a, Myc-CAP tumors (~200 mm^3) were treated with degarelix (ADT, 0.625μ*g*, *sc*), BMS`959 (N, 0.3 mg/kg, *it*) or their combination for 7 days. Harvested tumors were analyzed by flow cytometry to calculate frequency of PD-L1/CD86 expressing TAM within TME. **b**, Myc-CAP tumors (~200 mm^3) bearing mice were treated with indicated agent(s) either until non-palpable tumors for 4 weeks or until tumors reached euthanasia end-point (~2500 mm^3). In parallel, corresponding cohorts of mice received clodronate (200μg, *ip*, 1-hour pretreatment), to systemically deplete TAM, prior to administration of ADT, N and ADT/N. Survival curves were plotted for 60 days. **c**, Harvested tumors were analyzed by flow cytometry to quantify PD-L1/CD86 expressing TAM within TME. **d**, Schema represents primary or metastatic PC TME which have a predominance of immunosuppressive M2 TAM and a relative paucity of anti-tumor NLRP3-expressing M1 TAM. AR blockade (ARB) primes NLRP3 in the M2 TAM, and BMS`959 differentiates these NLRP3 primed M1/M2 TAM into PD-L1/CD86 expressing NPP TAM, which phagocytose cancer cells, resulting in tumor clearance. Data obtained from specimens of mice ($n \geq 3$ mice per group). Except panel **d**, All panels show biological replicates as mean $\pm$ s.e. Significances/p-values were calculated by two-way ANOVA (panel **a**, **c**), Kaplan-Meier survival analysis (panel **b**) and indicates as follows, *$p<0.05$, **$p<0.01$ and ***$p<0.001$; ns = not statistically significant. U = untreated tumors.